A compact bellows-driven diamond anvil cell for high-pressure, low-temperature magnetic measurements

Yejun Feng, D. M. Silevitch, and T. F. Rosenbaum

A compact bellows-driven diamond anvil cell for high-pressure, low-temperature magnetic measurements

Yejun Feng,[1,2] D. M. Silevitch,[2] and T. F. Rosenbaum[2]
[1]*The Advanced Photon Source, Argonne National Laboratory, Argonne, Illinois 60439, USA*
[2]*The James Franck Institute and Department of Physics, The University of Chicago, Chicago, Illinois 60637, USA*

We present the design of an efficient bellows-controlled diamond anvil cell that is optimized for use inside the bores of high-field superconducting magnets in helium-3 cryostats, dilution refrigerators, and commercial physical property measurement systems. Design of this non-magnetic pressure cell focuses on *in situ* pressure tuning and measurement by means of a helium-filled bellows actuator and fiber-coupled ruby fluorescence spectroscopy, respectively. We demonstrate the utility of this pressure cell with ac susceptibility measurements of superconducting, ferromagnetic, and antiferromagnetic phase transitions to pressures exceeding 8 GPa. This cell provides an opportunity to probe charge and magnetic order continuously and with high resolution in the three-dimensional Magnetic Field–Pressure–Temperature parameter space. © *2014 AIP Publishing LLC*. [http://dx.doi.org/10.1063/1.4867078]

I. INTRODUCTION

High-pressure science has been a vibrant research field for several decades, and many groups have presented impressive construction designs tailored to specific sample environments.[1–7] Among all high-pressure vessels, diamond anvil cells (DAC) are most commonly used due to the combination of a large accessible pressure range and a relatively compact structure. Although early designs could be cumbersome,[1,2] a contemporary full sized diamond anvil cell is typically 2 in. (50 mm) in diameter and 1–3 in. (25–75 mm) in height.[3] The essential elements of such a DAC consist of either cylindrical surfaces or pins to provide sliding alignment of the opposing anvils, seats and/or rockers for providing support and lateral and rotational alignment of the anvils, gaskets for maintaining a relatively homogeneous sample environment, access windows into the pressure chamber, and some method for applying force for sealing and pressurization. The pressurization method typically consists of Belleville disk springs, a split spring,[3,5] or a turnbuckle,[6,7] and possibly a lever arm[1] or a helium membrane/bellows actuator for *in situ* adjustment of the pressure.[4,8]

Miniature DAC systems have been developed with cross-sectional diameters under 9 mm[6,7] for magnetization measurements in the tight confines of a superconducting quantum interference device (SQUID) magnetometer. In order to fit the tight space constraints, the cell designs must simplify or eliminate many general components of a DAC system. In particular, the fine-tuning capability provided by both spring washer stacks (at room temperature) and a helium bellows system (under experimental conditions) have been sacrificed.

Motivated by the opportunity to probe Magnetic Field–Pressure–Temperature (*H-P-T*) phase space for the electronic and magnetic signatures of correlated electron states and related quantum phase transitions, we present here the design and characterization of a high-pressure diamond anvil cell that comfortably fits into the bore of most general-purpose superconducting magnets as well as high-field resistive and hybrid magnets.[9] The cell was designed with a maximum outer diameter of 1 in. (25.4 mm) for compatibility with the Physical Properties Measurement System (PPMS) line of cryostats from Quantum Design; this design rule also provides compatibility with a wide range of systems, including variable-temperature inserts designed for 32 and 50 mm magnet bores and helium-3 and dilution refrigerator systems with similar space constraints. Being intermediate in size between the two limits mentioned above, this cell is similar to a previous design,[4] but is slightly smaller in diameter and much simpler in construction. It preserves both spring washers and the helium membrane structure for continuous fine tuning of pressure without the need to thermally cycle to room temperature. The pressure cell is built out of non-magnetic materials in order to probe magnetism and superconductivity over a temperature range from milliKelvin to hundreds of Kelvin. We test the utility and sensitivity of this new DAC design by measuring for $0 < P < 8.5$ GPa the Meissner signal at the superconducting transition in Pb and the features in the ac magnetic susceptibility at the ferromagnetic and antiferromagnetic transitions in Dy.

II. CONSTRUCTION OF THE BELLOWS-CONTROLLED HIGH-PRESSURE CELL

We show in Fig. 1 the design and assembly of the diamond anvil cell. The body of the cell is made of silicon aluminum bronze (C64200). This material has a high strength and is non-magnetic and resistant to corrosion. Unlike BeCu, this bronze alloy does not require heat treatment and is more easily machined to the high precision required. It also has excellent anti-galling and anti-seizing characteristics under non-lubricated and vacuum conditions, which makes it very suitable for a high-pressure cell intended for pressure changes at cryogenic temperatures. This material has been
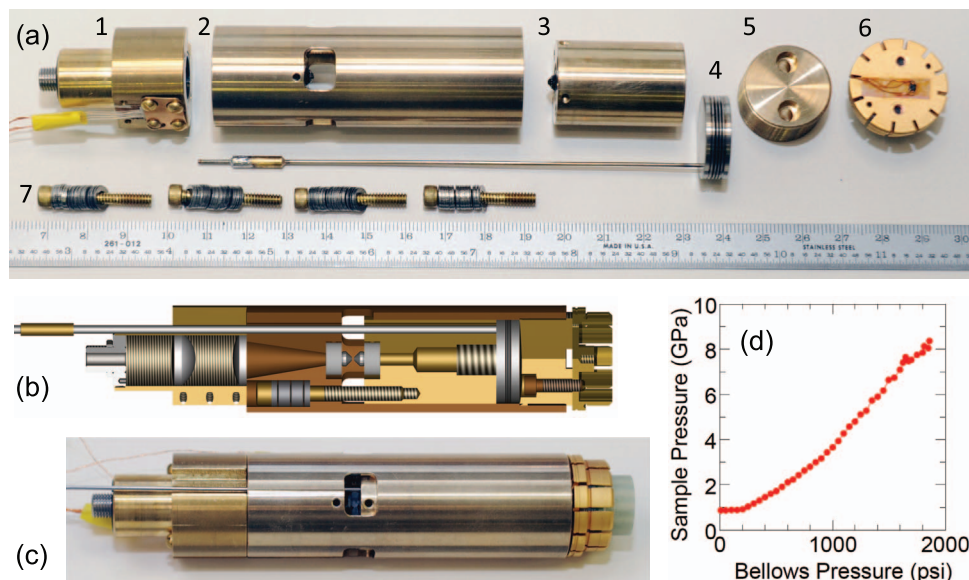
FIG. 1. Design of the compact bellows-controlled diamond anvil cell. (a) Disassembled cell showing individual components: (1) optics mount containing SMA fiber coupler and two plano-convex lenses to couple sample chamber to fiber; a Cernox thermometer is attached to the outside to measure the cell temperature. (2) Outer cylinder of the cell body. A mounted diamond is visible through the window. (3) Inner cylinder of the cell body with a second mounted diamond. (4) Helium bellows actuator. (5) Plug with external thread to screw into part 1 of the cell body for bellows confinement. (6) PPMS sample puck for mounting to cryostat base. A GaAs Hall sensor mounted to the puck measures the applied field. (7) Four brass 6-32 screws with stacks of 302 stainless steel Belleville spring washers (Associated Spring Raymond) for sealing and initial pressurization of cell. (b) Cross-sectional rendering of the internal structure of the cell. (c) Photograph of a fully assembled cell. (d) Loading curve of the bellows-actuator at $T = 8$ K. Pressure is measured using the ruby fluorescence through the fiber optics. Stick-slip motion of the cell is observed at high membrane pressures.

successfully used in the construction of helium membrane-controlled x-ray diffraction DACs.[8] The two opposing parts of the cell are aligned through sliding cylindrical surfaces. The cell is initially pressurized by four 6-32 screws tightened parallel to the cylindrical axis, and the rotational symmetry of the cell should not affect the cell alignment during pressurization. The length of the cell allows the use of stacked Belleville spring washers, which provide a gentle initial sealing and reduce the pressure variation that arises when cooling from room to cryogenic temperatures.

A key capability for efficiently studying materials at low temperature and under pressure is the ability to vary and measure the pressure without needing to warm the system to room temperature. In this DAC design, pressure tuning is enabled by incorporating a custom bellows actuator (316 stainless steel, BellowsTech Inc.) pressurized with helium via a capillary line connected to a room-temperature gas reservoir and manifold. The bellows sits below the pressure chamber in the cell assembly with the capillary line for pressurizing the bellows passing through an access hole in the cell body. The bellows is 21 mm (0.827 in.) in diameter and has been tested to 1800 psi of gas pressure; with a pair of 800 μm culet diamonds, this corresponds to a pressure range of approximately 7 GPa (Fig. 1(d)). Once the bellows is used to provide the majority of the pressure, the cell pressure was observed to be stable to ± 0.1 GPa over a large temperature range between 10 and 250 K. However, when the helium pressure in the actuator is above 450 psi, solidification of the helium occurs for $T < 5$ K, resulting in a change of cell pressure; at 6 GPa, this pressure change was measured to be 0.15 GPa.

The other half of the requirement for efficient low temperature operation is the ability to measure the pressure in

the cryogenic environment. We use the standard ruby fluorescence technique,[3,8] with a single multimode optical fiber carrying both the incident light and the emitted spectrum and a pair of 0.5 in. (12.7 mm) diameter plano-convex lenses providing a wide-aperture coupling between the fiber and the pressure chamber (Fig. 1(b)). This efficient coupling allows the cell pressure to be measured with incident light power in the tens or hundreds of μW range, minimizing any local heating that might occur during the measurement. Similarly, spectroscopic measurements such as fluorescence and inelastic scattering (Raman) are feasible.[3] Moreover, the open geometry of the cell permits the optical fiber to be replaced with free-space optical coupling for polarization-sensitive optical measurements, offering the potential for techniques such as the Magneto-Optic Kerr Effect (MOKE)[10] and microscopic imaging in both the infrared and the visible bands.

For the measurements described in Secs. IV and V, the pressure cell was loaded inside a commercial helium-4 cryostat (PPMS, Quantum Design) with a base temperature of 1.75 K and a 9 T magnet. The cell was fastened to a standard PPMS sample puck, which was then attached to the copper thermal block at the base of the sample chamber. Thermal linkage between the cell and the cryostat was primarily through this block and puck. For use in top-mounting systems such as typical helium-3 and dilution refrigerators, an alternate mounting scheme would employ attachment to the optical mount at the top of the cell. As such cryostats often incorporate 1.25 or 2-in. diameter magnet bores, the 1 in. diameter of this cell allows ample clearance for the necessary vacuum and radiation shields needed for sub-Kelvin operation. A calibrated Cernox thermometer located on the optical mount and a GaAs Hall sensor attached to the sample puck provided direct

measurements of the temperature and field at the sample position. Due to the mass and height of the cell, the thermal gradients inside the cryostat were significant, and hence a second thermometer (in addition to the PPMS system thermometer) was required to characterize these gradients and accurately determine the sample temperature. The Hall sensor sensed trapped flux and other hysteretic behavior of the 9 T solenoid magnet, important for studying materials such as Type I superconductors that are sensitive to small fields. With the exception of the wiring for the Hall sensor (which used the PPMS built-in sample wiring), all of the electrical, optical, and gas lines were brought up to room temperature through the sample chamber and passed out through hermetic feedthroughs.

III. AC SUSCEPTIBILITY MEASUREMENTS

In order to characterize the cell's performance, we present here ac susceptibility measurements of both superconductivity and magnetism. The pressure cell is equally well suited for electrical transport measurements[11] and infrared and visible light probes. We use the standard gradiometric mutual inductance coil technique for measuring the complex ac magnetic susceptibility, a technique that has been widely used in diamond anvil cells, with compensation coils located both outside[2, 12–15] and inside[12, 16] the sample chamber. Here we use an external coil design[2, 12–15] over so-called "designer anvils" that have the pickup coil lithographically patterned on diamond[17] or sapphire[18] anvils. The external compensation coil configuration provides several advantages: it is cheaper, it is built separately from the pressure cell and is modular for ease of assembly, it accommodates anvils of different culet sizes to access different pressure ranges for different

experiments and, finally, in case of anvil failure under pressure there is a high probability of recovering the coils.

We constructed our coils using 25 or 50 μm diameter insulated oxygen-free high purity copper wire (California Fine Wire Co.) wound inside a coil form machined out of fused, magnetic-impurity-free Hysol epoxy with a 150 $\pm$ 25 μm wall thickness. Using a coil form improves the mechanical robustness of the assembly, allows for a modular construction, and provides a high packing density of the coil wires to increase both measurement sensitivity and field uniformity. After winding, we encapsulated both the drive and pickup coils in Stycast 2850 FT epoxy (Emerson & Cuming Co.) to provide further structural support (Fig. 2). We used two types of coil configurations. The first design had the pickup coil wound closely around the culet to maximize the filling fraction of the sample.[2, 13–15] The drive coil was wound on a second form well away from the pickup (Figs. 2(b) and 2(f)). The second approach used a similar design for the pickup coil, but the drive was wound on the same form directly on top of the pickup coil (Figs. 2(c) and 2(g)). In the case of anvil failure, the drive coil of the first design (I) is not damaged, while the pickup coil might need to be replaced. The second design (II) provided a larger and more concentrated ac field, at the risk of both coils being potentially damaged by anvil failure. The pickup coils in both designs consisted of approximately 200 turns of 25 μm wire. The drive coil in design I had either 500 turns of 50 μm wire or 2000 turns of 25 μm wire; in design II it consisted of 1100–1400 turns of 25 μm wire.

The drive and pickup coils were nested coaxially adjacent to one anvil (Figs. 2(b) and 2(c)) with the pickup coil in the same plane as the sample under pressure. The drive coil had a thickness of 1.5 mm and a total height of 1.8 mm including the frame. In order to obtain a smooth susceptibility
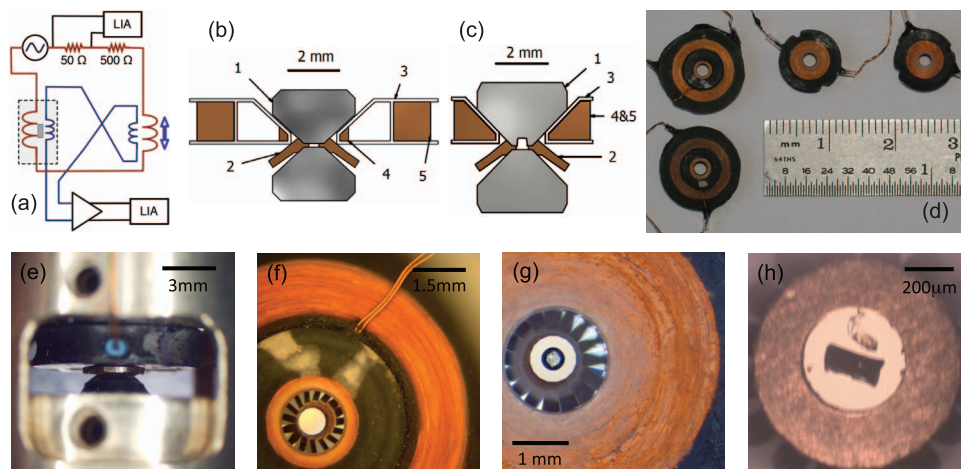

FIG. 2. AC susceptibility setup. (a) Electrical circuit diagram. The adjustable compensation coil set is placed outside of the cryostat (shaded area encircled by the dashed line). For the drive circuit (red), an ac voltage source is placed in series with measuring and current-limiting resistors, followed by the two drive coils. For the pickup circuit (blue), the two pickup coils are oppositely aligned and connected to a preamplifier. Lock-in amplifiers (LIA) synched to the voltage source read the voltage across the measuring resistor and the preamp output to determine the drive circuit current and pickup circuit voltage, respectively. (b) and (c) Cross-sectional view of two designs of susceptometer (I and II, respectively). The drive coil (5) is either in a separate coil form (3) away from the pickup coil (4) or directly wound outside of the pickup coil. In panel (c), one of the diamond anvils (1) has a partial perforation from the culet side to increase the sample chamber size. (d) Photograph of four coils with design I on the left and design II on the right, together with a ruler as a size marker. (e) Photograph of a fully assembled susceptometer, including gasket, diamond anvils, and coils, viewed through one of the windows of the high-pressure cell. (f) Top view of a coil of design I on top of a diamond anvil (800 μm culet size). (g) Top view of a coil of design II on top of a culet-perforated anvil. A metallic sample can be seen inside the partially perforated hole. (h) A typical view of the sample chamber for superconductivity measurements with both a Pb sample and a ruby manometer submerged in methanol:ethanol 4:1 mixture as the pressure medium inside the BeCu gasket.

background, we avoided using superconducting or magnetic materials around the coil and diamond anvils. The breakout leads were electrically connected to the coil wires by sandwiching both wires between Ag foil pads and binding them in place with silver epoxy; this yields a low contact resistance without mechanically stressing the thin coil wires.

Given that the mutual inductance between the drive and pickup coils tends to be large compared to the susceptibility of a magnetic sample, ac susceptometers are often constructed in a gradiometer configuration. In this geometry, a second set of coils wound in opposition null out the bulk of the mutual inductance signal (Fig. 2(a)). This is especially important for pressure-cell experiments given the typical small size of samples in the pressure chamber.[12, 15] In conventional ambient-pressure susceptometers, balancing is often achieved by constructing a second identical drive/pickup coil pair and placing it in the cryostat near the coil pair containing the sample so that thermal contraction and changes in impedance affect both sets equally. The tight space constraints of a pressure cell do not permit such *in situ* matching near the pressure chamber. Hence, it is difficult to wind a fixed coil that provides good compensation to the sample coil for a range of pressures and temperatures, especially since the mutual inductance of the sample coil is sensitive to changes in the gasket, pressure cell, and cryostat environments. Instead, we have fabricated a continuously adjustable coil set at room temperature (Fig. 2(a)).[12] The compensation system is composed of two coaxially nested cylindrical coils wound from 50 μm Cu wire whose relative position can be adjusted. Slightly moving the two coils with respect to each other changes their mutual inductance and thereby allows a tunable compensation for variable background signals from the sample coil set inside the cryostat. This nulling procedure is only valid for a single frequency at a time because the geometry of the compensation set differs from the sample coil set. In a typical measurement, we balance the two coil sets before the measurement starts with a background-nulled signal that is 0.25% of the original uncompensated response. As the background susceptibility signal primarily arises from the gasket, the compensation typically does not need to be further adjusted at every pressure.

AC susceptibility is typically measured using two dual-phase lock-in amplifiers (e.g., Stanford Research SR830 or Signal Recovery 7230), one to measure the current through the drive coil circuit and one to measure the voltage across the two pickup coils (Fig. 2(a)). For the latter, two voltage preamplifiers, a transformer-based unit (Stanford Research SR554), and an FET-based system with configurable band-pass filters (Stanford Research SR560) were tested using a 500× gain. The SR554 transformer preamp has a substantially lower noise floor for the low-impedance load of the pickup coil circuit; however, its gain depends strongly on circuit impedance, which can change by orders of magnitude between room temperature and base as the Cu coils cool, and its applicable frequency range may be too circumscribed for spectral interrogation of samples. The FET-based SR560, with its largely flat response as a function of frequency and input impedance, offers more flexibility and is more suitable for measurements spanning broad ranges in

temperature, at the cost of ∼10× higher noise floor in the final data.

The cell and support structure were constructed to minimize the use of ferromagnetic or superconducting materials around both the sample and coil sets. In addition to constructing the cell body from a nonmagnetic bronze alloy, we used non-magnetic seats for the diamond anvils such as single-crystal sapphire disks (Swiss Jewel Co.) and hot-pressed silicon nitride disks (Insaco Co.); typical tungsten carbide compounds are ferromagnetic due to the inclusion of cobalt as a binder. Furthermore, the use of electrically insulating seats helps to minimize eddy currents that heat the sample space and introduce a large imaginary χ'' in the measured susceptibility. The gaskets for the pressure chamber were made from BeCu shim stock (Alloy 25, Materion Brush Performance Alloys) with a cold-rolled hard temper and a 305 μm initial thickness. Round gasket blanks of 3.5 mm diameter were batch produced by a die punch. The gasket size was chosen to be 4–5 times the diamond culet size to minimize eddy currents yet still provide sufficient strength. The blanks were pre-indented to 120–130 μm thickness and the hole defining the pressure chamber was electrical discharge machined to 390–490 μm in diameter. The BeCu gaskets were heat treated to Rockwell C38 hardness by precipitation hardening.

IV. SUPERCONDUCTIVITY UNDER PRESSURE

A superconductor is a perfect diamagnet and the superconducting transition is marked by a change of $1/4\pi$ in the magnetic susceptibility (in cgs units). We use lead as our trial example of the evolution of the superconducting transition temperature with pressure. Pb is a type I superconductor with a critical temperature $T_c = 7.23$ K and a critical field $H_c = 802$ Oe at ambient pressure. A typical sample chamber assembly is shown in Fig. 2(h), where a piece of ruby and a thin slab of Pb (99.9999%, Cominco American Inc.) were surrounded by the 4:1 methanol:ethanol mixture used as a pressure medium. A probe ac field of 2 Oe, much smaller than the critical field H_c, was used. We plot in Fig. 3(a) the step in $\chi'(T)$ at the superconducting transition for several pressures up to 8.2 GPa. The width of the superconducting transition is 30 mK at $P = 2.5$ GPa; approximately 25 mK of the width can be ascribed to the finite response time of the lock-in amplifier's 3-s time constant convolved with the 100 mK/min temperature ramp rate. At 8.2 GPa, the transition width is approximately 75 mK, corresponding to a pressure inhomogeneity of 0.14 GPa across the sample dimensions. We note that this inhomogeneity is consistent with previous estimates[8] for a 200×100 μm^2 sized sample (Fig. 2(h)). The superconducting transitions in this DAC have comparable sharpness to those measured in a Bridgman anvil cell using a liquid pressure medium.[19] We trace in Fig. 3(b) $T_c(P)$ and, as expected, reproduce results found in the literature.[2, 19]

In addition to the transition temperature T_c, the critical field H_c is an important characteristic of the superconducting state. With the pressure cell able to fit inside a 50 mm bore superconducting magnet, we are able to probe the H-T phase diagram of a superconductor by either measuring $\chi'(H)$ at a fixed temperature (Fig. 3(c)), or measuring $\chi'(T)$ in a fixed
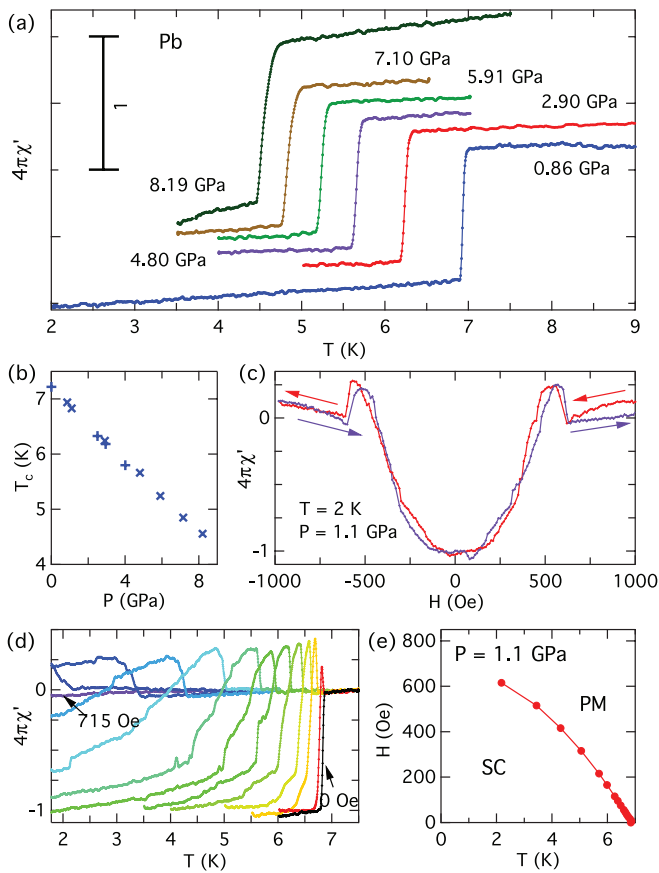
FIG. 3. (a) Change in the ac magnetic susceptibility with temperature, $\chi'(T)$, of Pb at its superconducting transition for six pressures P. Data are taken using a gradiometer configuration at frequency $f = 167.31$ Hz and an ac probe field of 2 Oe. The vertical bar represents 1 as the perfectly diamagnetic superconducting signal, and is approximately 3.7 nV at the pickup coil before amplification. Traces are vertically displaced for clarity. The larger step size in the 8.19 GPa trace is likely due to a flattened sample shape at that pressure. (b) $T_c(P)$ for two different samples. (c) Background-subtracted $\chi'(H)$ at $T = 2$ K and $P = 1.1$ GPa. Background was measured at 10 K for each pressure. Arrows indicate field ramp directions. (d) Representative $\chi'(T)$ curves at various static magnetic fields: 0, 6, 25, 45, 75, 115, 165, 215, 315, 415, 515, 615, and 715 Oe. All curves are displaced vertically to match at $T = 7$ K. At 4 Oe and above, the differential paramagnetic effect becomes visible. (e) The H-T phase boundary of superconductivity (SC) in Pb at $P = 1.1$ GPa with the transition temperature $T_c(H)$ extracted from panel (d).

external static magnetic field (Fig. 3(d)). For fixed fields above 4 Oe, $\chi'(T)$ develops a peak on top of the zero-field behavior; the perfect diamagnetic shielding also broadens significantly with increasing field. This increase in susceptibility is also seen in $\chi'(H)$ (Fig. 3(c)). This behavior represents the differential paramagnetic effect, which has been observed in elements,[20] alloys,[12,21] and high-T_c cuprates. We note that this differential paramagnetic effect was also unintentionally observed in previous pressure experiments on Pb in zero applied field,[22] suggesting that some components of that pressure cell, likely the tungsten carbide anvils, were ferromagnetic. In general, the onset of the peak in $\chi'(T)$ marks the superconducting transition temperature T_c. Using the measured $\chi'(T)$ at various H, we generated a H-T phase diagram of Pb at $P = 1.1$ GPa (Fig. 3(e)). $H_c(T = 0)$ for Pb is 802 Oe at ambient pressure. At 1.1 GPa, the projected $H_c(T = 0)$ is suppressed to 700 Oe.

V. FERROMAGNETIC AND ANTIFERROMAGNETIC TRANSITIONS UNDER PRESSURE

Both ferromagnetic and antiferromagnetic transitions exhibit features in the ac magnetic susceptibility that can be tuned with P.[14,17] As the signals tend to be smaller than those associated with superconducting transitions, additional techniques are needed to achieve a reasonable signal to noise ratio. Two previous approaches used either a SQUID-based detection scheme[14] or a pickup coil lithographically patterned onto a "designer anvil," thereby permitting a large filling fraction for the sample.[17] Here, we discuss a third technique, enhancing the signal by increasing the sample volume via culet-perforated diamond anvils (Figs. 2(c) and 2(g)). Surface perforation has been used widely in sapphire anvil cells[3] and has been applied to diamond anvils as well.[23] We use a culet perforation of 350 μm diameter and 300 μm depth on an 800 μm culet size Drukker type diamond anvil to measure the magnetic behavior of elemental dysprosium, which has a transition into an antiferromagnetic state at Néel temperature $T_N = 179$ K, followed by a transition into a ferromagnet at Curie temperature $T_C = 85$ K. The large moment (10.3 μ_B) of Dy, combined with a 10 times larger sample volume because of the perforated diamonds, provides good signal to noise. However, the perforated diamond technique with the expanded pressure chamber has potential drawbacks. It enhances the volumes of both the sample and the pressure medium, and for a highly compressible pressure medium such as 4:1 methanol:ethanol, the contraction of the medium leads to significant inward flow of the gasket material into the perforated hole, and a consequent risk of diamond failure. For the results reported here, a silicone oil with low compressibility was used instead as a pressure medium; we expect that further fine-tuning of the perforation and gasket parameters will allow use of media such as methanol:ethanol mixtures.

We used coils of design II for the ac susceptibility measurements; the close-packed drive coils allow 10 mA of current to generate 60 Oe at the sample position. Non-annealed, polycrystalline Dy samples (99.9%, Alfa Aesar) were shaped by razor blades into a cylindrical form of 250–300 μm diameter and 300 μm height (Fig. 2(g)). We plot in Fig. 4(a) the background-subtracted susceptibility at a range of pressures and temperatures from 10 to 200 K, as well as the empty-cell background. The temperature dependence of the background is due to changes in the resistivity of the metallic components of the cell and thermal expansion/contraction of pieces of the assembly relative to the coil. The variation of this background is sufficiently small that there is no need to adjust the compensation coil during temperature scans.

The characteristic susceptibility profiles[24] of both the antiferromagnetic transition (peak-like) at 180 K and the ferromagnetic transition (step-like, measured at the steepest point) around 85 K are seen clearly. Due to the polycrystalline nature of our Dy samples, the transition temperature is not as sharp as in single crystals,[24,25] but was similar to other measurements on polycrystalline samples.[17,26] We also observed a large temperature hysteresis ($\sim$20 K) in our samples as compared to the smaller hysteretic width ($\sim$3 K) observed for single crystals.[25]
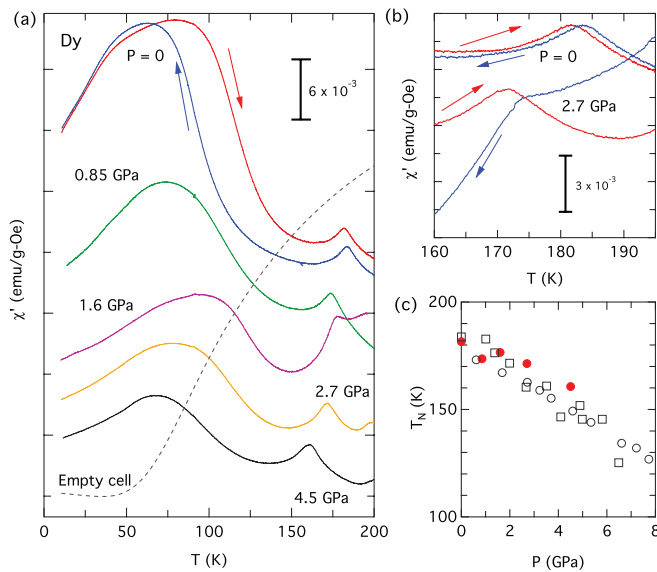
FIG. 4. Magnetic transitions in dysprosium under pressure. (a) ac suscep-tibility of Dy as a function of temperature for pressures ranging from 0 to 4.5 GPa after subtraction of a temperature-dependent background (dotted line). An antiferromagnetic transition is observed at $T_N(P=0) = 180$ K and a ferromagnetic transition at $T_C \sim 85$ K. For $P = 0$, both warming and cool-ing curves are plotted, showing a substantial thermal hysteresis in the sample between the strong first-order ferromagnetic to antiferromagnetic transition. For $P > 0$, only warming curves are plotted for clarity. (b) Warming and cool-ing curves for $P = 0$ and 2.7 GPa in the vicinity of T_N. The difference in T_N between warming and cooling is likely due to a thermal gradient between the sample and the thermometer as the antiferromagnetic to paramagnetic transi-tion is continuous. (c) The Néel temperature vs. pressure compared to values from Ref. 17 (open circles) and Ref. 26 (open squares).

Unlike the signature of the ferromagnetic transition, which is strongly affected by the demagnetization factor, the peak in χ' marking the antiferromagnetic transition can be used to estimate the measurement sensitivity of our suscep-tometer. The ambient-pressure antiferromagnetic transition in single-crystal Dy has $\chi'(T_N) = 5.0 \times 10^{-3}$ emu/g/Oe for H $\parallel$ $\boldsymbol{a}$, and 1.25×10^{-3} emu/g/Oe for H $\parallel$ $\boldsymbol{c}$, yielding an average of $\chi'(T_N) = 3.8 \times 10^{-3}$ emu/g/Oe for polycrystalline Dy.[24] With a sample mass of 0.13 mg and a measurement field of 60 Oe, this corresponds to a net measured signal of 3×10^{-5} emu. With the temperature dependent background of Fig. 4(a), our susceptometer is sensitive to magnetic signals that are a factor of 10 smaller. In order to achieve a higher sensitivity, it is pos-sible to place a compensation coil next to the sample coil so as to minimize the temperature dependent background.[12–15]

As the pressure is increased, T_N is suppressed by approx-imately 7 K/GPa (Fig. 4(c)), consistent with previous mag-netization/susceptibility measurements under high pressure[25] to $P \sim 7.7$ GPa.[17,26] The data spread in the three $T_N(P)$ phase boundaries of Fig. 4(c) are also presumably due to the use of polycrystalline samples of only 99.9% purity and non-annealed temper.

VI. CONCLUSIONS

We have designed and constructed a diamond anvil cell that is suitable for measurements inside 32 mm and 50 mm bore superconducting magnets typically found in helium-3 cryostats, dilution refrigerators, and commercial characteri-zation systems such as Quantum Design's PPMS. The cell allows *in situ* pressure tuning and measurement, using a he-lium bellows-controlled actuator and a fiber-coupled ruby spectrometer, respectively. We demonstrate the capabilities of the DAC via ac susceptibility measurements of both su-perconducting and magnetic transitions under pressure. The high-pressure cell, along with its components for sensing the magnetic susceptibility, are modular, economical, and easy to operate. This technology opens measurement capabilities for a broad swath of materials at extremes of temperature, pressure, and magnetic field.

[1] A. Jayaraman, Rev. Mod. Phys. **55**, 65 (1983).
[2] B. Bireckoven and J. Wittig, J. Phys. E: Sci. Instrum. **21**, 841 (1988).
[3] M. I. Eremets, *High Pressure Experimental Methods* (Oxford University Press, New York, 1996).
[4] R. J. Chen and B. A. Weinstein, Rev. Sci. Instrum. **67**, 2883 (1996).
[5] A. G. Gavriliuk, A. A. Mironovich, and V. V. Struzhkin, Rev. Sci. Instrum. **80**, 043906 (2009).
[6] G. Giriat, W. Wang, J. P. Attfield, A. D. Huxley, and K. V. Kamenev, Rev. Sci. Instrum. **81**, 073905 (2010).
[7] D. E. Graf, R. L. Stillwell, K. M. Purcell, and S. W. Tozer, High Pressure Res. **31**, 533 (2011).
[8] Y. Feng, R. Jaramillo, J. Wang, Y. Ren, and T. F. Rosenbaum, Rev. Sci. Instrum. **81**, 041301 (2010).
[9] J. R. Miller *et al.*, IEEE Trans. Magn. **30**, 1563 (1994).
[10] Z. Q. Qiu and S. D. Bader, J. Magn. Magn. Mater. **200**, 664 (1999).
[11] R. Jaramillo, Y. Feng, and T. F. Rosenbaum, Rev. Sci. Instrum. **83**, 103902 (2012).
[12] J. S. Schilling, S. Diederichs, S. Klotz, and R. Sieburger, in *Magnetic Sus-ceptibility of Superconductors and Other Spin Systems*, edited by R. A. Hein, T. L. Francavilla, and D. H. Liebenberg (Plenum Press, New York, 1991), pp. 107–128.
[13] C. C. Kim, M. E. Reeves, M. S. Osofsky, E. F. Skelton, and D. H. Lieben-berg, Rev. Sci. Instrum. **65**, 992 (1994).
[14] M. Ishizuka, K. Amaya, and S. Endo, Rev. Sci. Instrum. **66**, 3307 (1995).
[15] Y. A. Timofeev, H.-K. Mao, V. V. Struzhkin, and R. J. Hemley, Rev. Sci. Instrum. **70**, 4059 (1999).
[16] P. L. Alireza and S. R. Julian, Rev. Sci. Instrum. **74**, 4728 (2003).
[17] D. D. Jackson, V. Malba, S. T. Weir, P. A. Baker, and Y. K. Vohr, Phys. Rev. B **71**, 184416 (2005).
[18] O. P. Welzel and F. M. Grosche, Rev. Sci. Instrum. **82**, 033901 (2011).
[19] D. Jaccard and K. Sengupta, Rev. Sci. Instrum. **81**, 043908 (2010).
[20] R. A. Hein and R. L. Falge, Phys. Rev. **123**, 407 (1961).
[21] G. W. Hull, J. H. Wernick, T. H. Geballe, J. V. Waszczak, and J. E. Bernardini, Phys. Rev. B **24**, 6715 (1981).
[22] T. Nakanishi, N. Takeshita, and N. Môri, Rev. Sci. Instrum. **73**, 1828 (2002).
[23] K. Shimizu, H. Ishikawa, D. Takao, T. Yagi, and K. Amaya, Nature (Lon-don) **419**, 597 (2002).
[24] D. R. Behrendt, S. Legvold, and F. H. Spedding, Phys. Rev. **109**, 1544 (1958).
[25] H. Bartholin and D. Bloch, J. Phys. Chem. Solids **29**, 1063 (1968).
[26] M. Mito *et al.*, J. Phys. Chem. Solids **70**, 1290 (2009).